Molten Al and (0001) α-Al_2O_3 Single Crystal: Interface Stability

JOAQUIN AGUILAR-SANTILLAN

The roughness on the "*c*"-plane (0001) sapphire single crystal reduces wetting of molten aluminum under Ar gas (99.999 pct) and PO_2 10^{-15} Pa from 1073 K to 1473 K (800 °C to 1200 °C). The contact angle effect was partially understood by the roughness factor, ***R***; however, the interfacial phenomenon involving this effect is yet a topic to study as it also depends, between other things, on the shape of droplet and the relationship to its substrate. The theory explains that the surface tension of liquid aluminum obtained by the sessile drop test can be determined just when a substrate is polished or free of any surface imperfection. However, roughness of sapphire (0001) surface promotes an apparent surface tension that exhibits different trends of wetting to that proposed in previous studies. This property adds to the interfacial wetting phenomena obtained from the Al-Al_2O_3 couple system and provides answers for contact angle trends toward a much more stable interface, which when coupled with thermodynamic conditions may help in the manufacturing, deterioration, and reliability of the system.

DOI: 10.1007/s11661-016-3680-7

I. INTRODUCTION

THE correct measurements of interfacial phenomena such as surface tension, contact angle, and the work of adhesion between fluid interfaces with a restricting solid are of extreme importance to surface science research. These technology metrics are limiting new developments and technologies within materials science and metallurgy to its corresponding industry. Example of those challenges ranges from smaller scale semiconductors, packaging, and assembly by studying smaller and dissimilar materials to historical problems of metal interactions to refractories.[1–5]

Rough solid surfaces have a technologically important influence on the wetting of solid surfaces by liquids. Wenzel[4] was the first to recognize it on the wetting phenomenon of solid surfaces by liquids and defined the roughness factor ***R*** as follows:

$$\boldsymbol{R} = \text{Roughness factor} = \frac{\text{Actual surface area}}{\text{Geometric surface area}} > 1. \quad [1]$$

The value of ***R*** is greater than unity. The true surface area of a rough surface is greater than the geometric or projected surface area and also greater than that of a smoothly polished surface. A rough surface may also be structurally different than a smoothly polished one and that study still remains unclear.

A direct experimental approach is the sessile drop technique, which is shown schematically in Figure 1. When a pure liquid wets a smooth and chemically homogeneous surface of an inert solid, the wetting driving force at time t and temperature T can be expressed by Eq. [2]:

$$Fd(t, T) = \gamma_{sv} - \gamma_{sl} - \gamma_{lv} \cos \phi(t, T), \quad [2]$$

where the γ_{ij} are the characteristic interfacial surface tensions of the system and ϕ (t, T) is the instantaneous contact angle. At equilibrium, when $Fd = 0$ this leads to the classical Young equation[6,7]:

$$\cos \phi = \frac{\gamma_{sv} - \gamma_{sl}}{\gamma_{lv}}. \quad [3]$$

In principle, the absolute value of Eq. [3] could be used, but the functional evaluation and its characteristics for γ_{sl} and γ_{sv} have not been determined. Young's equation has been modified to include the solid roughness factor ***R*** as follows:

$$\cos \phi' = \frac{\boldsymbol{R}(\gamma_{sv} - \gamma_{sl})}{\gamma_{lv}} = R \cos \phi, \quad [4]$$

where ***R*** is the roughness factor as previously defined in Eq. [1] and ϕ' represents the contact angle for a rough surface. Equation [4] is known as Wenzel's equation. The apparent contact angle (ϕ') of a solid rough surface is ***R*** times higher than that of a flat or smoothly polished surface (ϕ).

It is evident that when a fluid interacts with a solid, the wetting contact angle (ϕ) changes by the presence of surface roughness effects. Surface chemistry effects may

JOAQUIN AGUILAR-SANTILLAN, R&D Director, formerly with the Metallurgical and Materials Engineering Department, University of Alabama, PO Box 870202, Tuscaloosa, AL 35407-0202, is now with Materials and Tools, LLC, 4118 East Washington Ct, Gilbert, AZ 85234. Contact e-mail: joaquin.aguilar@materialstools.solutions

Manuscript submitted August 25, 2015.
Article published online August 2, 2016

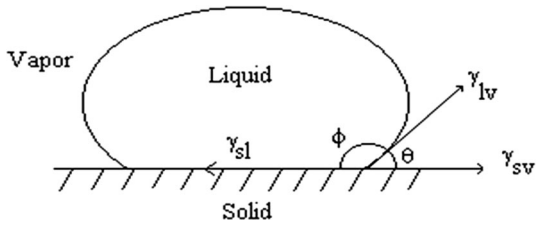

Fig. 1—Energy balance and the contact angle definition of Young's equation. Note the two different definitions of the contact angles, ϕ and θ.

also be important for specific solid–liquid systems and may dominate the wetting phenomena through reactive wetting processes of the solid by a liquid as described by Eustathopoulos *et al.*[1] Several nonreactive or inert liquid/solid systems have been recently studied within the concept of surface roughness effects;[8,9] however, no metrics have been studied on wetting phenomenon stability for a molten metal on a solid ceramic at elevated temperatures.

An important inert or nonreactive wetting system is that of molten aluminum on the solid ceramic alumina, Al_2O_3. The inert metal/ceramic couple of molten aluminum (Al) and alumina or aluminum oxide (Al_2O_3) is known to be stable at elevated temperatures because of the high formation energy of Al_2O_3, −1675.3 kJ/mol. However, the oxygen partial pressure is normally sufficiently high; a thermodynamic gas-forming reaction has been reported[1,10,11]:

$$8Al(l) + 3.5O_2(g) + Al_2O_3 = 5Al_2O_2(g).$$

This reaction is reported to have a large, negative free energy, $\Delta G_{933.15K} = -640.3$ kJ.

Wetting of aluminum oxide, Al_2O_3, by molten aluminum is offering some opportunities for further understanding. It is evident in the past decades contact angle studies of intrinsic and extrinsic properties such as surface roughness,[12] crystallographic orientation,[10] PO_2,[10,11,13–23] and measurement techniques[24] affect the system. Therefore, mechanism of wetting that governs such as interfacial phenomena based on interfacial surface energies is an opportunity. Thus, the objective of this work is to study the sapphire surface roughness effect (***R***) and its effects on the stability phenomena from the "apparent" liquid aluminum surface tension.

II. EXPERIMENTAL PROCEDURES

An optical grade (α-Al_2O_3) sapphire single crystal in the form of a disk (0.6 cm in thickness × 12.3 cm in diameter) and with a purity >99.996 pct was cut from a synthetic Czochralski-grown crystal boule purchased from commercial Lannyte Co. The disk was clear and transparent. The (0001) crystallographic plane was used to evaluate the effect of the surface roughness of sapphire on the wetting with the 1020 aluminum. The "c"-plane (0001) was used to study different surface roughnesses. Rough surfaces were produced by abrasion with an SiC paper of grit sizes of 220 (63 μm), 120 (102 μm), and 60 (254 μm) in the direction of the sapphire (0001) surface. A 0.5-μm diamond paste was used to produce the smoothly polished surface.

A Philips XL 30 scanning electron microscope (SEM) was used to characterize the polished and the abraded surfaces of sapphire single crystals. The surfaces were carbon coated through a sputtering device BioRad Polaron E6430. Secondary electrons, a voltage of 15 kV, and a spot size of 3.0 were the conditions used in the SEM for their surface observation.

The aluminum metal specimens for the sessile droplets were fabricated from a commercial Wrought 1020 Al alloy provided by Alcoa. They were fabricated to solid cylinders with a diameter and a height of 5 mm. The droplets weighed approximately 0.60 g each. Their volume in the molten state was about ~0.25 cm^3. To minimize oxidation during the preparation and testing, the specimens were semi-polished using a 400 grit SiC paper followed by ultrasonic cleaning in isopropanol.

Sessile drop experiments of this molten aluminum on the sapphire (0001) were performed using a commercial sessile drop apparatus by Centorr Associates Inc. It is schematically illustrated in Figure 2. Axisymmetric sessile aluminum droplets on flat oxide ceramics were produced at elevated temperatures for the experiments. It is a common experimental technique.

The sessile drop experiments were completed in an Argon gas atmosphere using high-purity Ar (99.999 wt pct) to minimize the formation of an alumina skin on the surface of the molten aluminum droplet. Results obtained by other investigators, even in a vacuum, often experienced aluminum oxidation because of the inadequate reduction of the oxygen partial pressure within the entire experimental system. It is recognized that there exists a problem of oxygen partial pressure that may cause an alumina skin to develop on the molten aluminum droplet. Previous researchers have considered this situation. As noted by John and Hausner,[16] a partial pressure of oxygen of less than 10^{-44} Pa at 973 K (700 °C) is necessary to avoid this problem. In practice, it is impossible to avoid some oxide formation on the aluminum droplet's surface. The degree to which it affects the measurement is not known with certainty, but most likely the effect can be minimized when the experiments are reproduced carefully.

The actual experiment consisted of placing the oxide substrate and the aluminum metal cylinders (0.5 × 0.5 cm) at the center of the furnace. After closing the furnace, a vacuum was applied to the level of 7 Pa. When this was reached, Ar ~ 99.9999 pct was introduced into the furnace through a valve at a furnace pressure of 130 Pa. This sequence was repeated four times to reduce the system's residual oxygen to a low level. Final wetting measurements were completed in Argon gas in the sessile drop furnace with the Argon at the tank pressure of ~104 Pa. The partial pressures of several gas species were $PH_2 = 10^{-14}$, $PH_2O = 10^{-16}$, $PN_2/CO = 10^{-17}$, and $PO_2 = 10^{-15}$ Pa as determined by a gas analyzer MKS Vision 100-B.

Temperature was controlled by increasing the current (mA) on the furnace heating element. Current was applied until the desired test temperature was reached. A

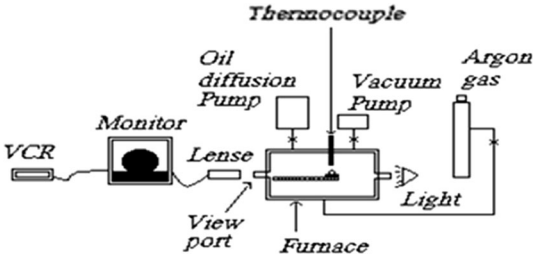

Fig. 2—Schematic of the sessile drop apparatus.

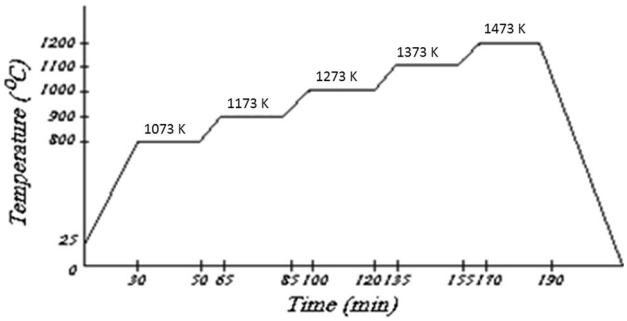

Fig. 3—Heating schedule followed in the sessile drop measurements.

typical heating schedule is illustrated in Figure 3. Experiments were completed in the intervals of 373 K (100 °C) at the temperatures from 1073 K to 1473 K (800 °C to 1200 °C) for a duration of 20 minutes at each temperature.

When the Al metal specimen was melted, it immediately formed an axisymmetric droplet on the ceramic substrate (~0.01 second). The experiments were video-recorded. A time duration of 20 minutes was used at each temperature. This period of time had been previously reported by Li[11] as the length of time at which the contact angle no longer changes for the molten aluminum/alumina system. Recorded videos of the sessile drop experiments were transferred to a PC memory using a hardware DFG/LC1 frame grabber and the Grab and View 2.1 software. This combination allows the observation of individual frames at any time (~0.001 second) during the experiment. The zero-time contact angle measurement taken in this study was the time at which the axisymmetric droplet shape forms completely on the ceramic substrate. This was determined by the image analysis in the intervals of time from 0.001 to 0.01 second. A sample image is illustrated in Figure 4.

III. RESULTS

The SEM micrographs in Figure 5 illustrate the polished sapphire (0001) surface and the three different rough (0001) surfaces created by SiC grit abrasion. The different surface conditions are evident. The 0.5-μm-diamond-polished surface appears very smooth, and by atomic force microscope analysis (AFM), the surface was shown to have an *Ra* mean of 200 nm and a

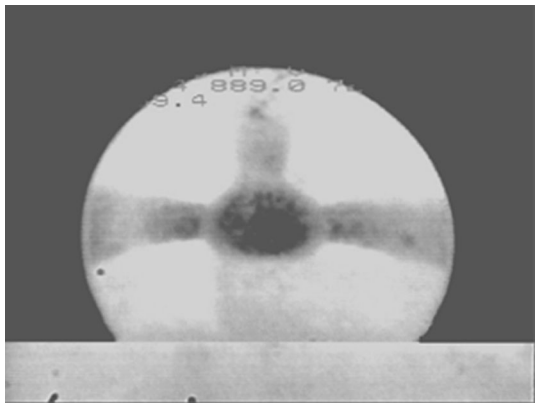

Fig. 4—A typical molten aluminum sessile droplet resting in sapphire at elevated temperature.

standard deviation of 35 nm. After abrasion with 220 grit SiC, the AFM shows an *Ra* mean of 56,000 nm and a standard deviation of 1856 nm. The coarse 60 grit SiC yielded large directional scratches with AFM showing an *Ra* mean of 254,060 nm and a standard deviation of 25,255 nm. The 120 grit SiC abrasion created an intermediate appearance to that of the 60 and 220 grit abrasions showing an *Ra* mean of 106,540 nm and a standard deviation of 10,858 nm.

The roughness on the "*c*"-plane (0001) sapphire single crystal increases the wetting contact angle of molten aluminum under Ar gas (99.999 pct) and PO_2 10^{-15} Pa from 1073 K to 1473 K (800 °C to 1200 °C). Previous work has extensively described the experimental procedure, metrology, data collection, capability analysis, and its control.[12,24] The studies have shown that temperature promotes a large difference in $\boldsymbol{R}_o$ values. Since the roughness factor changes linearly with temperature, the complete derivation of $\boldsymbol{R}$ (t, T) can be approximated by Eq. [5]:

$$\boldsymbol{R}' = \boldsymbol{R}'_o + (d\boldsymbol{R}'/dT)T, \qquad [5]$$

where $\boldsymbol{R}'_o$ represents the roughness factor at zero Kelvin.

IV. ALUMINUM SURFACE TENSION ON A SMOOTHLY POLISHED SAPPHIRE (0001) SURFACE

A. *The γ_{lv} (t, T)*

The present study focuses on the surface tension (γ_{lv}) of molten pure aluminum as determined by the numeric integration of the nonlinear (ODE) Laplace equation of capillarity to the sessile droplet shapes. The surface tension (γ_{lv}) of molten aluminum resting on the sapphire (0001) polished surface is presented in Figure 6 as a function of time at constant temperature, *i.e.*, $(d\gamma_{lv}/dt)_T$. This variation is apparently smaller than the temperature effect. The temperature promotes larger differences in the surface tension, γ_{lv}, of molten aluminum. This linear trend with respect to time can be derived as follows:

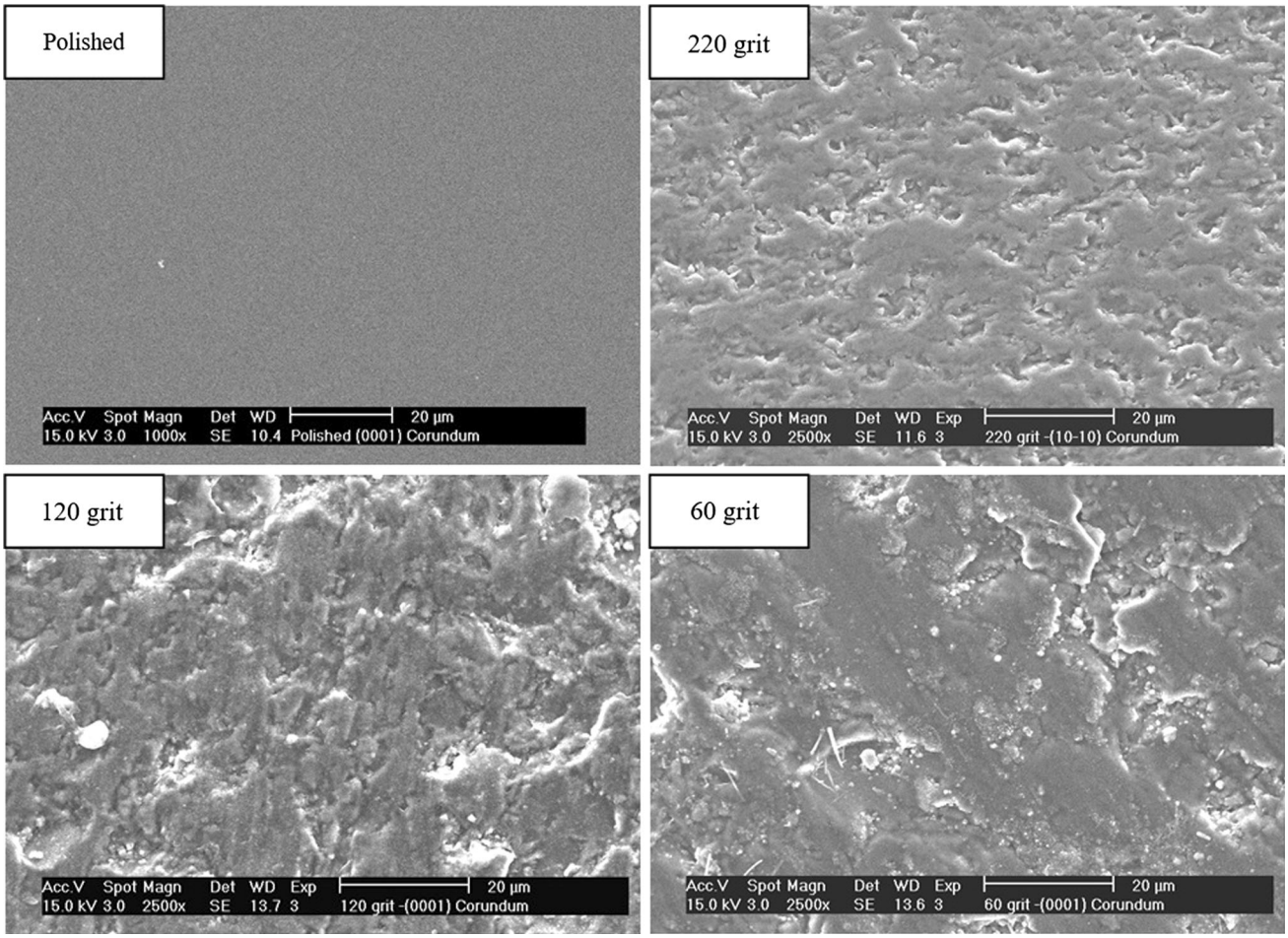

Fig. 5—SEM photographs of the (0001) surface of sapphire single crystal with different roughness levels. the polished surface (0.5 μm), the 220 grit surface (63 μm), the 120 grit surface (102 μm), and the 60 grit surface (254 μm).

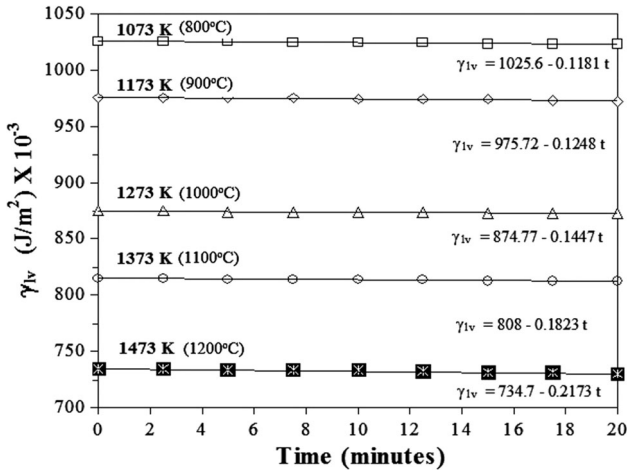

Fig. 6—Surface tension, γ_{lv}, variation with time at constant temperatures. Conditions for Al with sapphire (0001) plane polished surface.

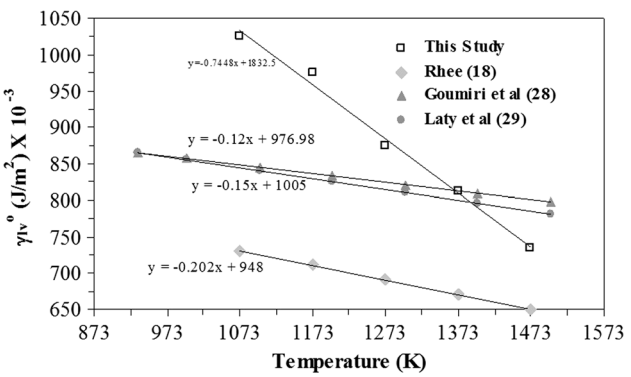

Fig. 7—Variation of γ_{lv}^{o} with temperature for aluminum on the polished sapphire (0001) surface. The results by Goumiri *et al.* and Laty *et al.* as well as Rhee are also illustrated.

$$\gamma_{lv} = \gamma_{lv}^{o} - (d\gamma_{lv}/dt)_T t, \qquad [6]$$

where γ_{lv}^{o} represents the surface tension at time zero and the slopes $(d\gamma_{lv}/dt)_T$ are observed to increase proportionally with the temperature also. The γ_{lv}^{o} changes with temperature are illustrated in Figure 7.

The temperature effect on the Al surface tension, γ_{lv}^{o}, shows a linear trend and its variability is compared with those reported in other research studies. For example, Rhee[18] reported the surface tension (γ_{lv}) of pure molten

Table I. Slopes, $(d\gamma_{lv}^{o}/dT)$ (J/m^2 K), Obtained in the Present Research and Those Obtained in the Literature

Researcher	Time (min)	Conditions/Roughness (μm)	$(d\gamma_{lv}/dT)$ (J/m^{2}K) $\times 10^{-3}$
Rhee	not reported	Al-AlN/(1)	−0.202
Laty *et al.*	not reported	Al-maximum bubble test	−0.150
Goumiri *et al.*	not reported	Al-maximum bubble test	−0.120
This study	zero	Al-sapphire (0001) / (0.5)	−0.745

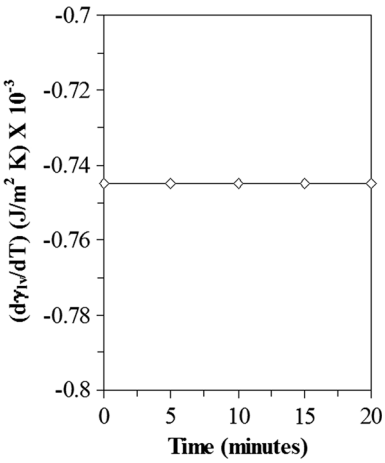

Fig. 8—Slope $(d\gamma_{lv}/dT)$ variation with time obtained during wetting of the polished sapphire (0001) surface by molten aluminum. Note that the interval duration of 20 min for the sessile drop experiment does not affect this property, $(d\gamma_{lv}^{o}/dT)$.

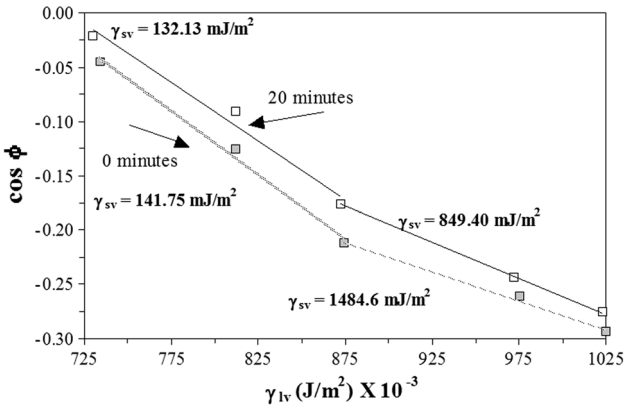

Fig. 9—Variation of cos ϕ with surface tension (γ_{lv}). This analysis allows one to calculate $\gamma_{cs} = \gamma_{sv}$ at spreading condition, *i.e.*, $\phi = 0$. Note the different spreading solid surface energies, γ_{sv}, because of the slope change at 1273 K (1000 °C).

aluminum on AlN substrate, and the results by Goumiri *et al.*[25] and Laty *et al.*[26] are for aluminum measured by the technique of the maximum bubble pressure. The surface tension values reported by Rhee are slightly lower than the values observed in the present study and also lower than those reported in the studies by Goumiri *et al.* and Laty *et al.* However, the linear trend and the correlation with temperature reported in our study were found to be similar to those reported in the latter studies. The general agreement of surface tension and their negative slopes with increasing temperature are evident (Table I and also represented in Figure 7) :

$$\gamma_{lv}^{o} = \gamma_{lv}^{o\prime} - (d\gamma_{lv}^{o}/dT)_T, \qquad [7]$$

where $\gamma_{lv}^{'o}$ represents the surface tension at the intersection of zero Kelvin. The $d\gamma_{lv}^{o}/dT$ functionality is defined by the droplet entropy $(\Delta S) = -(d\gamma_{lv}/dT)_{p,\mu}$ at constant pressure and at equilibrium chemical potential. The values of surface tension (γ_{lv}) always decrease with increasing temperature having negative slopes not much impacted by time (Figure 8), as defined by the third law of thermodynamics. Therefore, we can conclude that surface tension, γ_{lv}, is influenced as a function of γ_{lv} (T) and its derivation can be given as follows:

$$\begin{aligned} d\gamma_{lv} &= (d\gamma_{lv}/dt)_T dt + (d\gamma_{lv}/dT)_t dT \text{ or } d\gamma_{lv} \\ &= (d\gamma_{lv}/dt)_T dt + (d\gamma_{lv}^{o}/dT). \end{aligned} \qquad [8]$$

B. *The cos ϕ (γ_{lv})*

The graphical analysis of the last derivation can be observed if the cos ϕ data are plotted against surface tension (γ_{lv}) at constant times, zero and 20 minutes for comparison. This is illustrated in Figure 9. It is observed that the variation of cos ϕ with surface tension (γ_{lv}) is linear and it shows a deviation point at 875 mJ/m^2 at 1273 K (1000 °C). The variations between the time profiles of zero and 20 minutes reflect small differences; however, the surface tension (γ_{lv}) ranges largely from 725 to 1025 mJ/m^2.

The slopes of $(\delta\cos\phi/\delta\gamma_{lv})_t = -(\gamma_{sv} - \gamma_{sl})/\gamma_{lv}^2$ can be used to determine the critical surface tension or the solid surface energy $\gamma_{cs} = \gamma_{sv}$ at spreading condition as cos ϕ = 1.[27] This calculation is summarized in Table II and the spreading surface solid energy (γ_{sv}) is illustrated in Figure 9, as a function of time.

The hypothetic variation of the solid surface energy, γ_{sv}, has two regimens at $T < 1273$ K (1000 °C) and at $T > 1273$ K (1000 °C).[28–33] However, its variation with time reflects that differences are evident. The regime at $T < 1273$ K (1000 °C) has an intercept of a linear regression of 119 mJ/m^2 and a slope of 0.50 mJ/m^2. The regime at $T > 1273$ K (1000 °C) has an intercept of a linear regression of 1540 mJ/m^2 and a slope of −32.84 mJ/m^2 min. The solid surface energy, γ_{sv}, scalar values and changes are larger at high temperatures

Table II. Spreading Solid Surface Energy (γ_{sv}) Obtained by Interpolation at Spreading Condition

Temperature Transition (K)	Time (min)	$\cos\phi^0\gamma^{lv}$ (deg)	$(\delta\cos\phi/\delta\gamma_{lv})_t$ (deg m^2/mJ)	$\gamma_{cs} = \gamma_{sv}$ (mJ/m^2)
<1273 K (1000 °C)	20	1.2114	−0.0016	132.13
<1273 K (1000 °C)	0	0.8299	0.0012	141.75
>1273 K (1000 °C)	20	0.4054	−0.0007	849.43
>1273 K (1000 °C)	0	0.2577	0.0005	1484.60

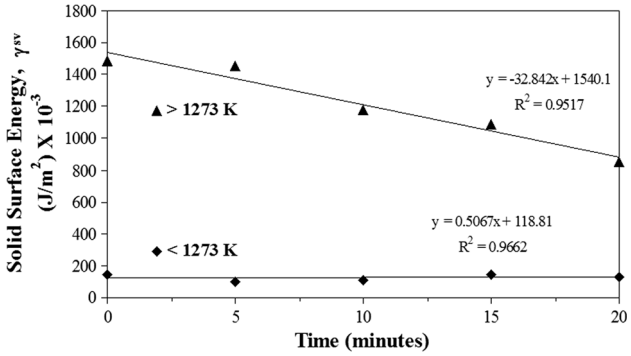

Fig. 10—Spreading solid surface energy, γ_{sv}, variation with time at spreading condition, *i.e.*, $\phi = 0$.

>1273 K (1000 °C). Also the differences between both regimes of variation are reduced as time increases as illustrated in Figure 9, defining the degree of equilibrium of the interface.

Figure 10 illustrates the changes of spreading solid surface energy, γ_{sv}, with time linearly in the interval from zero to 20 minutes. The slope $(\delta\gamma_{sv}/\delta t)_{T_{cs}}$ at constant spreading temperature, T_{cs}, is negative in the regime of $T > 1273$ K (1000 °C) and is positive in the regime of $T < 1273$ K (1000 °C). This can be written as

$$\gamma_{cs} = \gamma_{sv} = \gamma_{cs}^{0t} - (\delta\gamma_{sv}/\delta t)_{T_{cs}} \text{ for } T > 1273 \text{ K } (1000\,^{\circ}\text{C}) \quad [9]$$

$$\gamma_{cs} = \gamma_{sv} = \gamma_{cs}^{0t} + (\delta\gamma_{sv}/\delta t)_{T_{cs}} \text{ for } T < 1273 \text{ K} (1000\,^{\circ}\text{C}). \quad [10]$$

Here γ_{cs}^{0t} represents the spreading solid surface energy, γ_{sv}, at zero time. This analysis suggests that the spreading solid surface energy, γ_{sv}, shows a larger level of instability at the regime of $T > 1273$ K (1000 °C) than that for $T < 1273$ K (1000 °C).

V. ALUMINUM SURFACE TENSION ON A ROUGH SAPPHIRE (0001) SURFACE

A. *The γ_{lv}' (t, T)*

The apparent surface tension (γ_{lv}') of molten aluminum resting on roughened sapphire (0001) surfaces is presented in Figure 11 as a function of time at constant temperature, *i.e.*, $(\delta\gamma_{lv}'/\delta t)_T$. The results illustrate similar

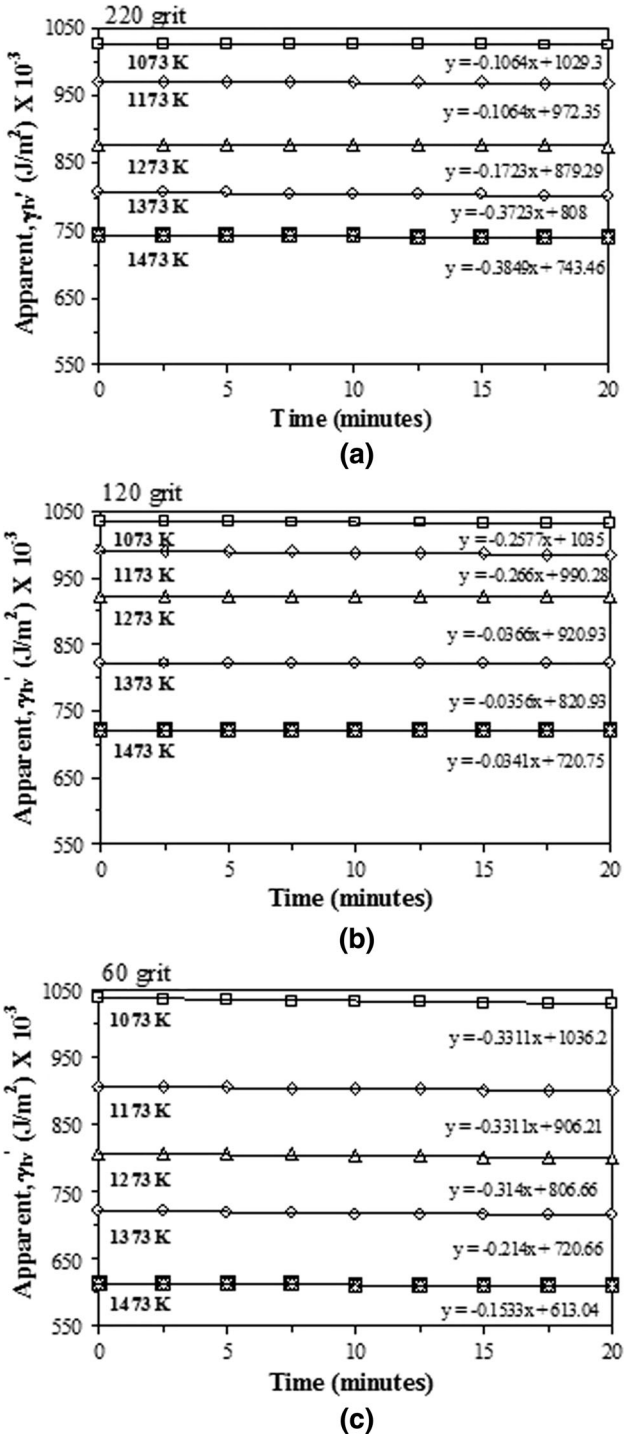

Fig. 11—Apparent surface tension, γ_{lv}', variation with time at constant temperatures for the roughened sapphire (0001) surfaces: 220 grit surface (*a*), 120 grit surface (*b*), and 60 grit surface (*c*).

linear variations. This derivation is mathematically equal for a roughened surface as previously defined for a polished sapphire (0001) surface, as follows:

$$\gamma'_{lv} = \gamma'^{0t}_{lv} - (\delta\gamma'_{lv}/\delta t)_T dt. \quad [11]$$

Here γ'^{0t}_{lv} represents the apparent surface tension at zero time.

The slopes $(\delta\gamma'_{lv}/\delta t)_T$ are presented in Figure 12 as a function of temperature. The slope changes are observed as "nucleation steps" showing activation mechanisms to promote wetting changes with a transition point at 1273 K (1000 °C). This is easy to recognize to align from previous work on contact angles[12] and well-studied sapphire structural transition at 1273 K (1000 °C).[34,35] The 220 grit surface changes negatively as slopes move from −0.10 to −0.38 mJ/m^2 min at 1073 K and 1473 K (800 °C and 1200 °C), respectively. The 120 grit surface reduced these slopes to similar negative values from −0.034 to −0.26 mJ/m^2 min, respectively. However, the 60 grit surface changes slopes to the contrary trend from −0.33 to −0.15 mJ/m^2 min, respectively. This suggests that apparent surface tension is influenced toward equilibrium with much rough sapphire (0001) surfaces and that it may help in processing of the interface. This in other words suggests that sapphire (0001) structurally changes at 1273 K (1000 °C)[34,35] and that roughness

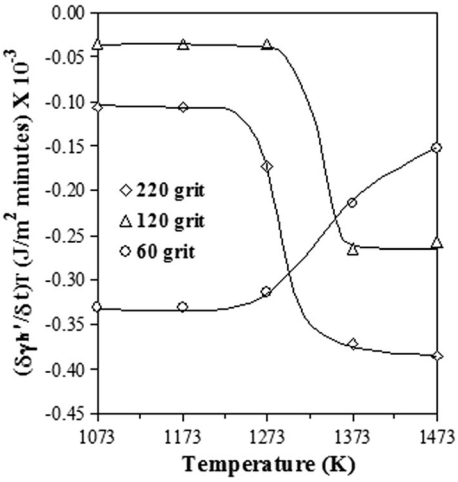

Fig. 12—Slope, $(\delta\gamma'_{lv}/\delta t)_T$, variation with temperature for the three roughened sapphire (0001) surfaces.

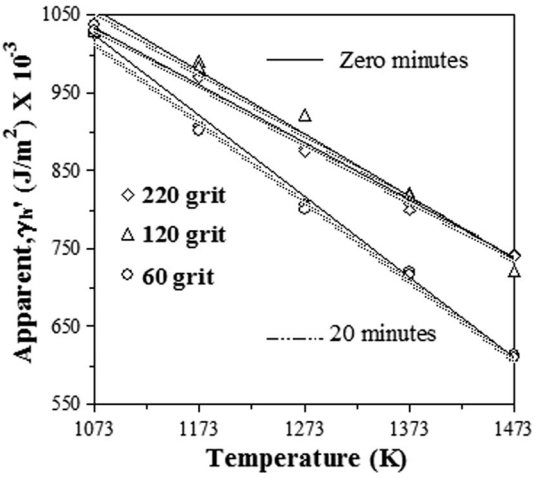

Fig. 13—Apparent surface tension (γ'_{lv}) of aluminum variation with temperature at constant times, zero and 20 min.

Table III. Wetting Analysis of the Roughened Sapphire (0001) Surfaces by Molten Aluminum

T_{cs} (K)	$T < 1273$ K (1000 °C)			$T > 1273$ K (1000 °C)		
Time (min)	220 Grit	120 Grit	60 Grit	220 Grit	120 Grit	60 Grit
0	5350.8	4209.4	4100.0	2356.4	1946.0	1929.9
5	5178.8	4170.0	4085.8	2220.6	1940.0	1920.0
10	5000.2	4169.4	4072.8	2150.0	1933.7	1914.0
15	4780.0	4155.8	4072.8	2100.9	1928.4	1908.0
20	4500.0	4104.4	4046.8	2000.0	1927.9	1900.0

Table IV. Slopes, $(\delta\gamma_{lv}'/\delta T)_t$ (J/m^2 K), Obtained with the Roughened Sapphire (0001) Surfaces

Surface (Grit)	Time (min)	Conditions/Roughness (μm)	$(\delta\gamma'_{lv}/\delta T)_t$ (J/m^2 K) × 10^{-3}
220	20	Al-sapphire (0001)/(63)	−0.736
	0		−0.744
120	20	Al-sapphire (0001)/(102)	−0.799
	0		−0.784
60	20	Al-sapphire (0001)/(254)	−1.035
	0		−1.025

levels impact the droplet geometry of the interface and may help stabilize the system (Tables III, IV).

Figure 13 illustrates the temperature effect on the apparent surface tension, γ_{lv}', for 0 and 20 minutes, and Figure 14 and Table V illustrate the slope variation of the apparent surface tension, γ_{lv}'/dT. Both show no obvious "nucleation steps" as those seen in Figure 12.

The roughness factor, $\boldsymbol{R}$, is plotted against the apparent surface tension, γ_{lv}', for times of 0 to 20 minutes in Figure 15 to illustrate the dependency of the apparent surface tension, γ_{lv}, on this property. The roughness effect on the apparent surface tension, γ_{lv}', is clearly visualized toward fewer slope values as roughness increases. These results suggest that the slope $(\delta\gamma_{lv}/\delta\boldsymbol{R})_t$ is reduced negatively with increasing time as follows:

$$\gamma_{lv}' = \gamma_{lv}^{\prime 0R} - (\delta\gamma_{lv}'/\delta\boldsymbol{R})_t d\boldsymbol{R}, \qquad [12]$$

and that its total derivation is obtained by taking the derivative as follows:

$$d\gamma_{lv}' = (\delta\gamma_{lv}'/\gamma t)_T dT + (d\gamma_{lv}'/dT)dT + (\delta\gamma_{lv}'/\delta\boldsymbol{R})_t d\boldsymbol{R}. \qquad [13]$$

Equation [13] explains the relationships and applies for the wetting of either sapphire (0001) polished surface or roughened sapphire (0001) surface.

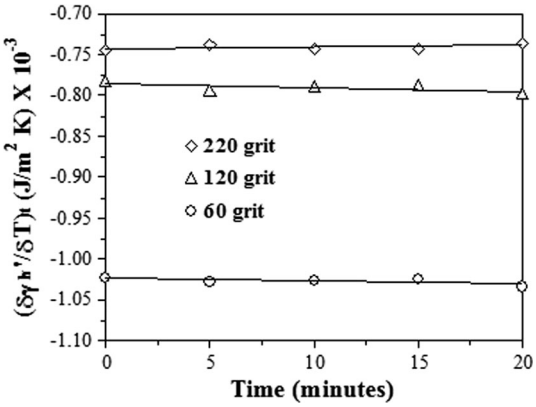

Fig. 14—Slope $(\delta\gamma_{lv}'/\delta T)_t$ variation with time obtained during the wetting of roughened sapphire (0001) surfaces by molten aluminum.

B. *The cos ϕ' (γ_{lv}')*

The graphical analysis of the cos ϕ' data *vs* the apparent surface tension (γ_{lv}') at constant time of 20 minutes is illustrated in Figure 16. It is observed that the variation of cos ϕ' with the apparent surface tension (γ_{lv}') is linear and it also shows that deviation points are obtained at 1273 K (1000 °C).[12] These points decrease linearly in the abraded surface order of 220, 120, and 60 grits. The variations between the time profiles from zero to 20 minutes in each abraded sapphire (0001) surface reflect small differences in the intervals of apparent surface tension (γ_{lv}') from ~600 to ~1050 mJ/m^2. The slopes of $(\delta\cos\phi'/\delta\gamma_{lv}')_t = -(\gamma_{sv}' - \gamma_{sl}')/\gamma_{lv}'^2$ can be used to determine the apparent critical surface tension, γ_{cs}', or apparent surface solid energy, γ_{sv}', at spreading conditions, *i.e.*, $\phi' = 0$. These calculations are summarized in Figure 17.

The variation of the apparent spreading solid surface energy, γ_{sv}', has the same regimens at $T < 1273$ K (1000 °C) and at $T > 1273$ K (1000 °C). However, γ_{sv}' variation with time reflects constant trends, but differences are evident between the two regimes for each roughened sapphire (0001) surface. The regime at

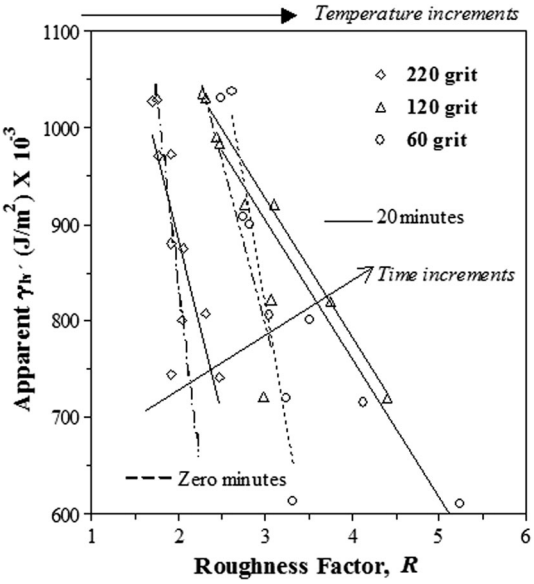

Fig. 15—Variation of the apparent surface tension, γ_{lv}', with the roughness factor, $\boldsymbol{R}$, for different time profiles of zero and 20 min.

Table V. Apparent Spreading Solid Surface Energy (γ_{sv}') Obtained by Interpolation at Spreading Condition, *i.e.*, $\phi = 0$

Transition T	<1273 K (1000 °C)			>1273 K (1000 °C)		
Time (min)	220 Grit	120 Grit	60 Grit	220 Grit	120 Grit	60 Grit
0	237.6	211.8	168.1	1085.7	1111.9	2045.0
5	241.6	225.7	159.0	1155.1	1152.3	1978.5
10	255.1	237.1	163.9	1069.9	1145.4	1974.0
15	278.4	227.3	171.2	1047.6	1030.4	1965.3
20	281.9	229.1	193.4	1054.0	978.5	1974.7

$T > 1273$ K (1000 °C) shows that γ'_{sv} is larger for the 60 grit surface (~2000 mJ/m^2) than those for 120 grit (~1130 mJ/m^2) and 220 grit (~1070 mJ/m^2) surfaces. This value suggests why the rougher surface promotes a most stable interface.

Figure 17 illustrates the changes of apparent spreading solid surface energy, γ'_{sv}, with time linearly in the interval of 20 minutes. The slope $(\delta\gamma_{sv}/\delta t)_{T_{cs}}$ at constant spreading temperature, T_{cs}, is negative in the regime of $T > 1273$ K (1000 °C) and is positive in the regime of $T < 1273$ K (1000 °C). This can be derived as follows:

$$\gamma_{cs} = \gamma'_{sv} = \gamma'^{0t}_{cs} - (\delta\gamma'_{cs}/\delta t)_{T_{cs}} \text{ for } T > 1273 \text{ K} (1000\,^{\circ}\text{C}) \quad [14]$$

$$\gamma_{cs} = \gamma'_{sv} = \gamma'^{0t}_{cs} + (\delta\gamma'_{cs}/\delta t)_{T_{cs}} \text{ for } T < 1273 \text{ K } (1000\,^{\circ}\text{C}). \quad [15]$$

Here γ'^{0t}_{cs} represents the apparent spreading solid surface energy, γ_{sv}, at time zero.

VI. DISCUSSION OF RESULTS

Differences in the previously reported results and those from the present work substantiate two principal surface effects:

(i) One is from the results when the surface energy of the solid is altered and wetting is directly affected by the surface energy of the solid, γ_{sv}, such as for the formation of new stable oxides at high partial pressure of oxygen at the triple contact line affecting the solid surface by reactive wetting (Eq. [1]). Brennan and Pask[10] have reported these Al-O compounds at high partial pressures of oxygen (10^{-3} to 10^{-4} Pa). The oxygen partial pressure is critical to the stability of the solid Al_2O_3 surface energy.

Levi *et al.*[15] have reported the liquid Al and sapphire wetting mechanisms under vacuum (10^{-3} Pa) and at different partial pressures of oxygen (10^{-7} and 10^{-9} Pa). They proposed two different mechanisms of wetting by microstructural examination, one at $T < 1373$ K (1000 °C) and the other at $T > 1373$ K (1000 °C). The mechanism at $T < 1373$ K (1100 °C) is suggested to be an epitaxial growth of new α-Al_2O_3 layers on the sapphire substrate and the mechanism at $T > 1373$ K (1100 °C) is suggested to be dissolution of the sapphire substrate. However, the results of the contact angle measurement obtained by Shen *et al.*[22] agree with those of Levi *et al.*: First, the transition temperature of the sapphire (0001) surface reported by Shen *et al.* is 1373 K (1100 °C), which is the same value as obtained by Levi *et al.* at a high partial pressure of oxygen. Second, Shen *et al.* reported to have worked at vacuum of about ~10^{-4} Pa, but they did not report the remaining partial pressure of oxygen. However, considering Levi *et al.* vacuum pressure of ~10^{-3} Pa, then it is possible that Shen *et al.* worked with almost the same experimental

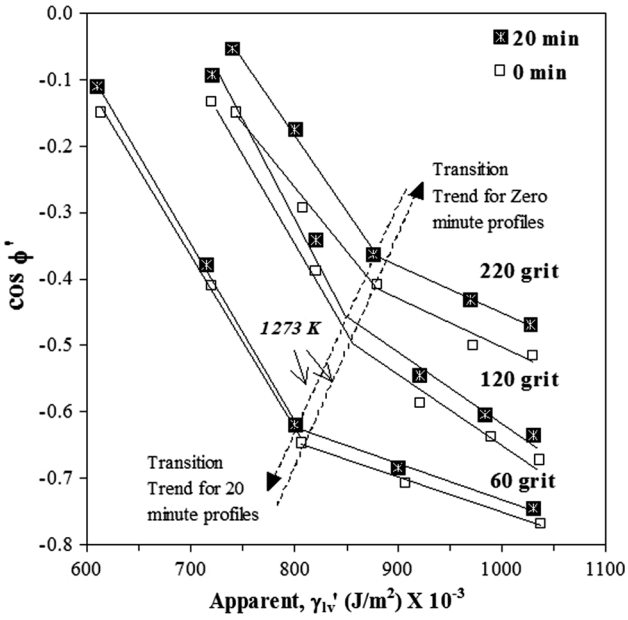

Fig. 16—Variation of cos ϕ' with the apparent surface tension, γ'_{lv}, for two constant times, zero and 20 min, and the three roughened sapphire (0001) surfaces.

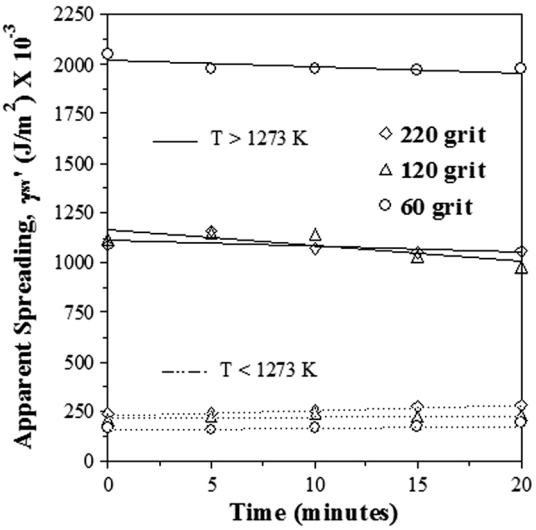

Fig. 17—Apparent spreading solid surface energy, γ'_{sv}, variation with time at spreading condition, *i.e.*, $\phi' = 0$. Note the differences of γ'_{sv} in the regimes of $T < 1273$ K (1000 °C) and $T > 1273$ K (1000 °C).

conditions. If this assumption is true, then the results of Shen *et al.* obey the mechanisms proposed by Levi *et al.* as a reactive wetting mechanism.

(ii) The second process is for apparent surface tension (γ'_{lv}) which controls the wetting phenomenon as reported in this study. It is influenced by the solid roughness effect. The slope changes are obtained between 1173 K and 1473 K (900 °C and 1200 °C) mainly by two steps of temperature showing activation mechanisms to promote wetting changes. The 220 grit

surface changes more negatively as slopes move from -0.10 to -0.38 mJ/m^2 K at 1073 K and 1473 K (800 °C and 1200 °C), respectively. The 120 grit surface reduced these slopes to similar negative values from -0.034 to -0.26 mJ/m^2 K, respectively. However, the 60 grit surface changes slopes to the contrary trend from -0.33 to -0.15 mJ/m^2 K, respectively. This measurement suggests that apparent surface tension stabilizes the wetting of 60 grit surfaces more than those of 220 and 120 grit surfaces. This is also true by analyzing the spreading solid surface energy where much more stable solid surfaces are developed.

The above facts represent the experimental low partial pressure of oxygen, ~10^{-15} Pa. In other words, this suggests that limited to no reaction occurs at the interfaces of Al liquid–vapor and sapphire–Al liquid or at least there is a very low probability of reaction because of the very low partial pressure of oxygen. Diffusion is still possible; however, it may be localized to high-chemical potential areas as most sessile parts tested in the experiments could separate mechanically without any external force at room temperature.

VII. SUMMARY AND CONCLUSIONS

The following show merit of the present findings:

The wetting of the α-Al_2O_3 (0001) single crystal surface by molten aluminum of 99.999 pct purity was experimentally studied from 1073 K to 1473 K (800 °C to 1200 °C) by the sessile drop technique. The sapphire (0001) surface was prepared in smoothly polished condition and also roughened through abrasion with increasing SiC grits (220, 120, and 60 mesh).

Interfacial engineering of aluminum and sapphire (0001) is summarized as a nonwetting system from 1073 K to 1473 K (1000 °C to 1200 °C) at PO_2 10^{-15} Pa. However, the variables such as time, temperature, and roughness play an important role in its nonwetting behavior. The aluminum surface tension varies with time and temperature to negative values, and when sapphire (0001) solid roughness increases (*i.e.*, level of 60 grit surface), changes are much more controlled and interface interactions promote wetting instead, $T > 1273$ K (1000 °C). Differences in localized crystalline structure and Al-O terminations are possible which are reported elsewhere to affect the surface tension mechanism; however, practical and manufacturing engineering composites may be considering additionally a controlled change by the roughness effect at elevated temperatures >1273 K (1000 °C).

ACKNOWLEDGMENTS

The author (J.A-S) would like to mention special thanks to Dr. Richard C. Bradt, and Dr. Doru Stefanescu from the University of Alabama for their mentorship and guidance throughout this study.

REFERENCES

1. N. Eustathopoulos, M.G. Nicholas, and B. Drevet: *Wettability at High Temperatures. Pergamon Materials Series*, Pergamon Press, New York, 1999, vol. 3, pp. 120–222.
2. B. Chalmers: *Principles of Solidification*, Krieger, Melbourne, 1982, pp. 20–122.
3. D.E. Clark and B.K. Zoitos: *Corrosion of Glass, Ceramics, Ceramics Superconductors*, Noyes, Park Ridge, 1991, pp. 21–78.
4. R.N. Wenzel: *Ind. Eng. Chem.*, 1936, vol. 28 (8), pp. 988–94.
5. W.D. Kingery, H.K. Bowen, and D.R. Uhlmann: *Introduction to Ceramics*, Wiley Interscience, New York, 1976, p. 372.
6. T. Young: *Philos. Trans. R. Soc. Lond.*, 1805, vol. 95A, pp. 65–67.
7. A. Dupre: *Theorie Mecanique de la Chaleur, Chapter IX, Actions Moleculaires (Suite)*, Pub. Gauthier-Villars, Paris, 1869, p. 87.
8. H. Nakae, R. Inui, Y. Hirata, and H. Saito: *Acta Mater.*, 1998, vol. 46 (7), pp. 2313–18.
9. Z. Yoshimitsu, A. Nakajima, T. Watanabe, and K. Hashimoto: *Langmuir*, 2002, vol. 18, pp. 5818–22.
10. P. Shen, H. Fujii, T. Matsumoto, and K. Nogi: *Acta Mater.*, 2003, vol. 48, pp. 779–84.
11. J.G. Li: *Ceram. Int.*, 1994, vol. 20, pp. 391–412.
12. J. Aguilar-Santillan: *Metall. Mater. Trans. A*, 2010, vol. 41A, pp. 686–88.
13. J.W. Nowok: *Mater. Sci. Eng.*, 1997, vol. A232, pp. 157–62.
14. X.B. Zhou and J.Th.M. De Hosson: *Acta Mater.*, 1996, vol. 44 (2), pp. 421–26.
15. J.J. Brennan and J.A. Pask: *J. Am. Ceram. Soc.*, 1968, vol. 51 (10), pp. 569–73.
16. H. John and H. Hausner: *Int. J. High Technol. Ceram.*, 1986, vol. 2 (1), pp. 73–78.
17. V. Laurent, D. Chatain, C. Chatillon, and N. Eustathopoulos: *Acta Metall.*, 1988, vol. 36 (7), pp. 1797–1803.
18. S.K. Rhee: *J. Am. Ceram. Soc.*, 1970, vol. 53 (7), pp. 386–89.
19. G. Levi and W.D. Kaplan: *Acta Mater.*, 2002, vol. 50, pp. 75–88.
20. D.J. Wang and S.T. Wu: *Acta Metall. Mater.*, 1994, vol. 42 (12), pp. 4029–34.
21. K. Landry and N. Eustathopoulos: *Acta Mater.*, 1996, vol. 44 (10), pp. 3923–32.
22. J.A. Champion, B.J. Keene, and J.M. Sillwood: *J. Mater. Sci.*, 1969, vol. 4 (1), pp. 39–49.
23. P. Shen, H. Fujii, T. Matsumoto, and K. Nogi: *Scr. Mater.*, 2003, vol. 48, pp. 779–84.
24. J. Aguilar-Santillan: *Metall. Mater. Trans. B*, 2009, vol. 40B, pp. 377–79.
25. L. Goumiri, J.C. Joud, and P. Desre: *Surf. Sci.*, 1979, vol. 83, pp. 471–86.
26. P. Laty, J.C. Joud, and P. Desre: *Surf. Sci.*, 1977, vol. 89, pp. 508–20.
27. W.A. Zisman: *Ind. Eng. Chem.*, 1963, vol. 55 (10), pp. 18–38.
28. J. Ahn and J.W. Rabalais: *Surf. Sci.*, 1997, vol. 388, pp. 121–131.
29. T.M. French and G.A. Somorjai: *J. Phys. Chem.*, 1970, vol. 74 (12), pp. 2489–95.
30. I. Manassidis and M.J. Gillan: *J. Am. Ceram. Soc.*, 1994, vol. 77 (2), pp. 335–38.
31. A. Marmier, A. Lozovoi, and M.W. Finnis: *J. Eur. Ceram. Soc.*, 2003, vol. 23, pp. 2729–35.
32. P.W. Tasker: *Surfaces of Magnesia and Alumina in Advances in Ceramics*, American Ceramic Society, Westerville, 1983, vol. 10, pp. 176–89.
33. P. Hartman: *J. Cryst. Growth*, 1989, vol. 93 (3), pp. 667–72.
34. E.A. Soares, M.A. Van Hove, C.F. Walters, and K.F. McCarty: *Phys. Rev. B*, 2002, vol. 65, pp. 195405–413.
35. T. Suzuki, S. Hishita, K. Oyoshi, and R. Souda: *Surf. Sci.*, 1999, vol. 437, pp. 289–98.